Liquid Crystals
Publication details, including instructions for authors and subscription information:
http://www.informaworld.com/smpp/title~content=t713926090

Flow of a liquid-crystalline polymer solution around an obstacle

Edith Peuvrel[a]; Patrick Navard[ab]
[a] Centre de Mise en Forme des Matériaux, [b] Ecole Nationale Supérieure des Mines de Paris, Valbonne, France

To cite this Article Peuvrel, Edith and Navard, Patrick(1990) 'Flow of a liquid-crystalline polymer solution around an obstacle', Liquid Crystals, 7: 1, 95 — 104
To link to this Article: DOI: 10.1080/02678299008029196
URL: http://dx.doi.org/10.1080/02678299008029196

LIQUID CRYSTALS, 1990, VOL. 7, NO. 1, 95–104

Flow of a liquid-crystalline polymer solution around an obstacle

by EDITH PEUVREL and PATRICK NAVARD†
Centre de Mise en Forme des Matériaux, URA CNRS 1374

(*Received 6 June 1989; accepted 26 June 1989*)

The behaviour of an anisotropic solution of hydroxypropylcellulose around an obstacle is investigated in shear and during relaxation. Experiments were carried out with an optical rheometer equipped with transparent cone-and-plate. The obstacle is a 200 micron glass sphere stuck on the plate. A typical Reynolds number past the obstacle is about 10^{-5}. The flow of the anisotropic solution perturbed by the obstacle shows specific phenomena: distorted downstream streamlines, a very long wake behind the obstacle during shear which persists a long time after the ceasing shear, a change in the behaviour at very high shear rates and in particular, the appearance of a wake in front of the obstacle. To date there has not been any theoretical bases with which to explain these new findings. An interesting point is that the wake behind the obstacle is a good illustration of the problem of weldlines in injection moulding.

1. Introduction

The rheology of liquid-crystalline main chain polymers is an interesting and current problem. Many investigations have been carried out with both thermotropic and lyotropic polymers [1–6], mainly focusing on steady state and relaxation of shear flows. Several new and puzzling phenomena were observed, related to the coupling between the velocity and stress fields and the director, and also due to the complex behaviour of the many defects present in liquid-crystalline polymeric samples. In the present study, we will report the results obtained when a liquid-crystalline polymer flows around an obstacle. To our knowledge, no work has been yet reported on such a subject, despite its relevance for example to the injection moulding of thermotropic polymers. Our purpose will be first to compare liquid-crystalline polymers to more classical fluids.

Hydroxypropylcellulose solutions were chosen as anisotropic fluids, mainly because experiments can be performed at room temperature, their rheology is reasonably well-known [7–11] and several rheo-optical studies have been carried out [12–17]. The present study will be only experimental since no theory can fully describe the rheology of such an anisotropic polymer, making any comparison between our results and theory very difficult. In the §§3 and 4, we will recall the rheo-optical properties of anisotropic hydroxypropylcellulose solutions and the behavior of different fluids past a circular cylinder. Phenomena occurring during the shear and relaxation of anisotropic hydroxypropylcellulose solutions past an obstacle will then be presented and discussed.

† Ecole Nationale Supérieure des Mines de Paris, Sophia-Antipolis, 06560 Valbonne, France.

2. Experimental

Most experiments with viscous or visco-elastic fluids are performed with a large tank and a long cylinder in order to avoid boundary effects. The cylinder (or the fluid) is moved, in order to have a fluid with an uniform velocity flowing around a fixed cylinder. In all cases, the observations are performed through a large fluid thickness. This is impossible with liquid crystals since they are very turbid. Thus the experimental set-up will be based on a transparent cone-and-plate rheometer, described elsewhere [15]. The cylinder will be simulated by a 200 μm glass sphere stuck on the plate, the glue filling the space below the sphere. It is important to keep in mind that the flow is much more complex than in the tank-cylinder case. Figure 1 shows the different axes with regard to the sphere. With the cone moving and the plate being fixed, there is a velocity gradient, even without an obstacle. Assuming a linear velocity profile and a laminar flow [18], we can compute a shear rate from the cone velocity. Shear rates between 1 s^{-1} and 190 s^{-1} were investigated. Chaotic instabilities occurred above approximately 190 s^{-1}. The experimental geometry is such that in addition to the flow around the sphere in the xy plane (figure 1), which is what will be observed since the observation axis is along the z axis, the polymer will also flow above the sphere.

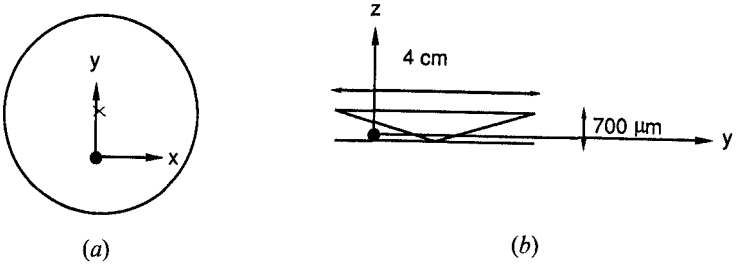

Figure 1. Location of the obstacle (black dot) in the cone-and-plate geometry. (*a*) Top view. (*b*) Gap view.

Three hydroxypropylcellulose (Hercules Klucel)-water solutions (M.w. = 60 000, 40 per cent by weight, isotropic; 50 per cent by weight, anisotropic; and M.w. = 100 000, 55 per cent by weight, anisotropic) were prepared using the usual procedure [15], except that a few per cent was filled with well-calibrated polystyrene spheres (diameter 9·89 μm, National Bureau of Standards reference material no. 1960). The spheres were used as velocity tracers. We checked that the moving spheres did not perturb the flow and could be considered as moving at the same speed as the surrounding fluid [18]. In these conditions, the Reynolds number was very low, about 10^{-5}.

3. Flow around a cylinder

As previously stated, the flow around a long cylinder is the closest simple analogy to our experimental geometry. Newtonian fluids have been extensively studied both experimentally and numerically [19–22]. At Reynolds numbers (Re) smaller than 5, the flow is laminar and streamlines are symmetrical around the cylinder (figure 2 (*a*)). Increasing Re begins to generate twin counter-rotating vortices, and at Re approximately 30, the wake becomes oscillatory. When Re approaches 70, von Karman vortices take place. Viscoelastic fluids have been less well studied [23–29] since

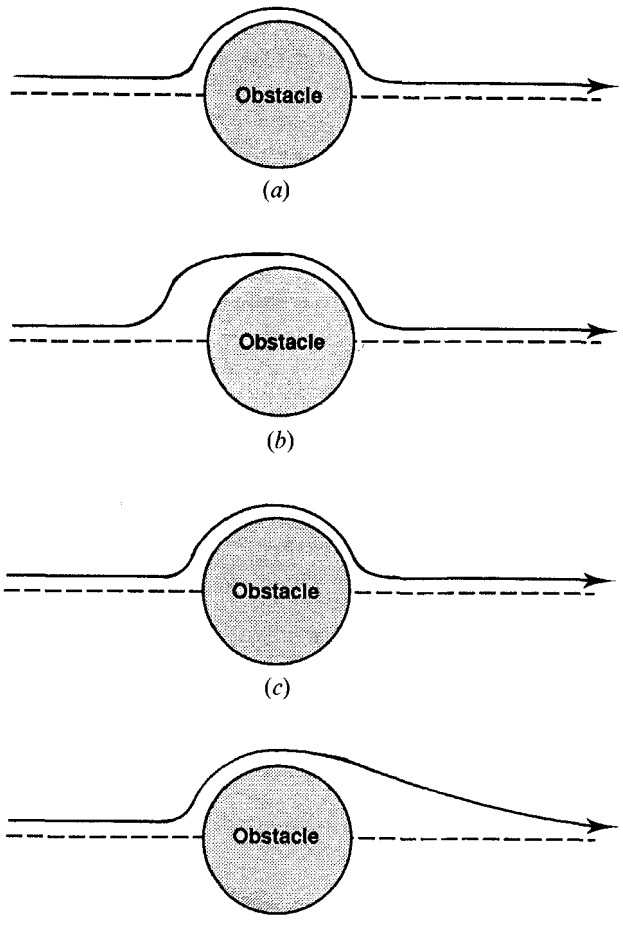

Figure 2. Schematic drawing of the streamlines for a uniform fluid past an obstacle at low Reynolds number. (*a*) Newtonian fluid (circular cylinder). (*b*) Viscoelastic fluid (circular cylinder). (*c*) Isotropic HPC solution. (*d*) Anisotropic HPC solution.

experiments, theories and numerical computations are far more difficult. Computations have been restricted to low and moderate Reynolds numbers. These show that the flow is laminar at low Re, but the streamlines are not symmetrical, as shown in figure 2(*b*). Most of the experiments have been carried out with dilute polymer solutions, and thus at low Weissenberg number. As expected, a small amount of polymer drastically modifies the flow. The stagnation point, located on the cylinder surface up to Re equals 0·4, is moved upstream with increasing Re. The cylinder is surrounded by a wide zone within which the fluid velocity is very small or zero. The distortion of the streamlines as in figure 2(*b*) predicted by the theory, has also been observed [23].

4. Results and discussions

Before describing the results it is necessary to summarize what is known about the flow and the relaxation of anisotropic hydroxypropylcellulose (HPC) solutions. Flow curves can be divided into two main regions [16]. At low shear rates, the texture seen

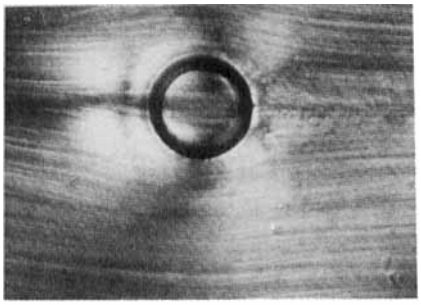

(*a*)

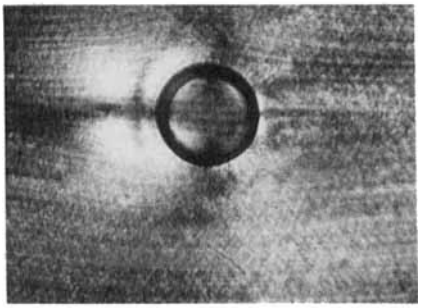

(*b*)

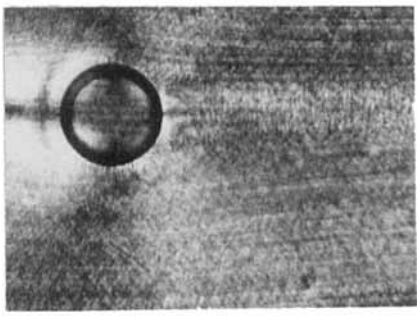

(*c*)

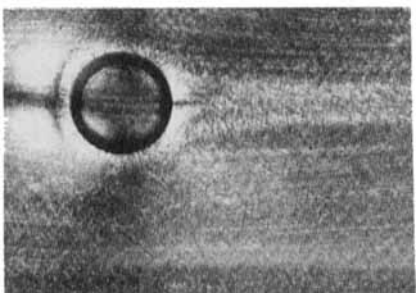

(*d*)

Figure 3. Optical micrographs taken at a low shear rate: $\dot{\gamma}_{xz} = 0{\cdot}3\,s^{-1}$. (*a*) During the shear. After stopping the flow, micrographs taken at different times: (*b*), (*c*), (*d*).

at rest is not drastically perturbed by the shear. Small angle light scattering (S.A.L.S.) and optical microscopy show that many defects are present and randomly dispersed. Upon relaxation, no special feature appears. Above a certain critical shear rate, for large deformations, the behavior is completely different. S.A.L.S. and optical microscopy give patterns and images which suggest the formation of particular supramolecular organizations [15–17]. Upon relaxation, a band texture appears, formed by a periodic orientation distortion of the molecules around the flow direction (x axis) and in the xy plane [15].

In the present study, the fluid was set into movement by the rotation of the cone, which generated a shear in the xz plane (the shear rate is $\dot{\gamma}_{xz}$). The results for the anisotropic solutions can be divided into three regions having different textural states of the fluid depending on the velocity of the cone.

4.1. *Isotropic solution*

Experiments were first carried out with an isotropic HPC solution. Streamlines were observed by using a solution filled with tracers. It was clear that, at low shear rates (tracers cannot be followed above $4\,s^{-1}$ [18]) streamlines are symmetrical in the isotropic solution (figure 2(*c*)). This is in contrast with experiments reported for solutions of long flexible chains [23].

4.2. *Anisotropic solutions: low cone velocity* ($\dot{\gamma}_{xz} < 1{\cdot}1\,s^{-1}$)

In this region, the texture due to the xz shear is very close to the texture at rest [16]. The observations were conducted using a polarizing microscope under crossed polar conditions, the analyser being parallel to the x axis. Figures 3(*a*) and 4 show what is observed in this region. Streamlines can easily be seen as long black lines. The origin of these lines is not clear. It was also possible to observe the streamlines by using a solution filled with tracers. Both methods give the same result: the streamlines are distorted downstream as shown in figure 2(*d*). This is a new result, since such a distortion at low Reynolds number has never been reported for any other fluid. The flow is laminar everywhere around the obstacle, and there is no vortex behind the obstacle that may explain this distortion.

Besides the four lobe birefringent zone that can be seen in figures 3(*a*) and 4, two other features can be observed. Some small black lines are present on the rear of the

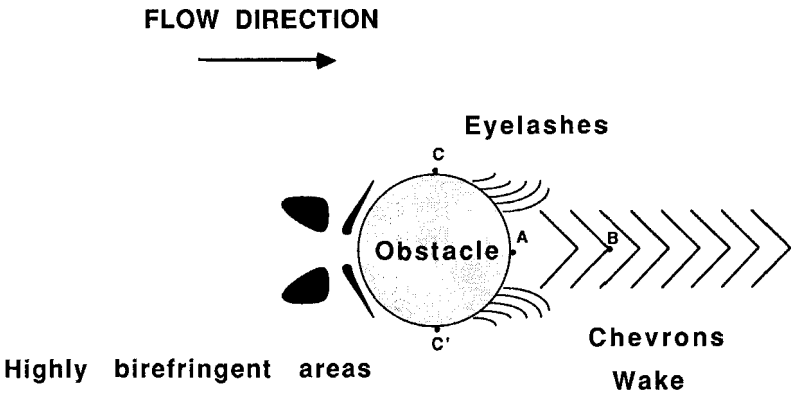

Figure 4. Schematic view of the shear at a low shear rate.

obstacle; these will be called eyelashes. These lines are also seen when the analyzer is removed. When a tracer particle goes through an eyelash region, it is slowed down and pushed away from the obstacle. Another interesting result is that a wake is formed behind the obstacle. The wake is large and very long. Just behind the obstacle, the wake has a texture which looks like chevrons (figures 3 (*a*) and 4). When the analyser is removed, the chevrons are not seen and the wake has a very small length. When a tracer or an air bubble goes straight onto the obstacle, it is first slowed down, then accelerated when bypassing around the obstacle, then slowed down in the eyelash region, and strongly accelerated in the wake to obtain the velocity of the surrounding fluid. The acceleration in the wake does not occur just after the obstacle. The velocity is small between point *A* and *B* of figure 4 and then the acceleration occurs. The fluid experiences alternate compressions and elongations as it passes around the obstacle. An important point to notice is that all the observed features are located at the same level in the *z* direction as the obstacle. Above it, none of the described phenomena is seen.

After ceasing the flow, no band should appear in the field of view due to the *xz* shear since the corresponding $\dot{\gamma}_{xz}$ is too small [15]. Nevertheless, bands appear around the obstacle and in the wake. The sequence of events is illustrated in figures 3 (*b*), (*c*), (*d*) and 5. Just after stopping the flow, eyelashes relax and seem to become the first black lines. These bands then propagate toward the front of the obstacle so that a corona of black lines (bands) builds up all around the obstacle, except just behind it. In the meantime, the chevrons disappear in the wake, and black lines (bands) appear there. The bands around the obstacle and in the wake, as shown in figure 5, remain a long time. The bands are present all along the wake over a large distance (up to 20 times the obstacle diameter), showing the extremely good orientation and mechanical memory of this fluid. This band texture has the same properties as the band texture appearing after a shear [15]. The only problem is that the *xz* shear is not large enough to produce a band texture. But since the velocity at the obstacle surface is zero, there is also a shear in the *xy* plane. Modelling the flow as if the fluid is pseudoplastic, and using the proper rheological and geometrical parameters, it is possible to evaluate the location and magnitude of this *xy* shear. The maximum shear is located at the *C* and *C'* points (figure 4). For a cone velocity corresponding to a uniform $\dot{\gamma}_{xz} = 0{\cdot}4\,\mathrm{s}^{-1}$, the $\dot{\gamma}_{xy}$ at point *C* or *C'* (near the eyelashes) is $2{\cdot}3\,\mathrm{s}^{-1}$, which is larger than the critical shear rate and so can generate band textures. The problem here is that the shear is not in the right plane. If we recall, shearing in the *xz* plane would produce bands seen in the *xy* plane. For the corona, the shear and the bands are in the same plane. As far as the wake is concerned, there is no shear of sufficient magnitude to produce a band texture. It is known that a relaxation after an elongation can produce a band texture

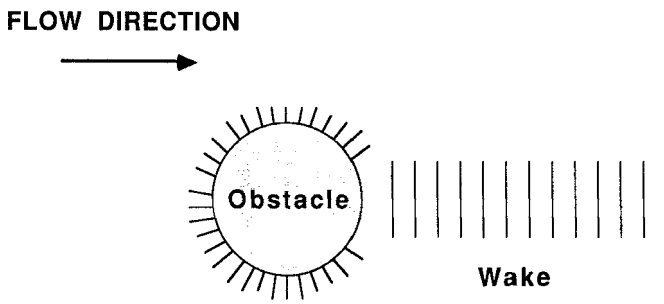

Figure 5. Schematic view showing what is observed after stopping the flow at a low shear rate.

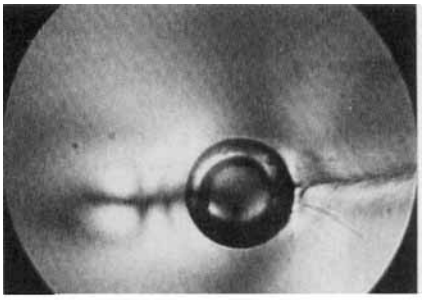

(*a*)

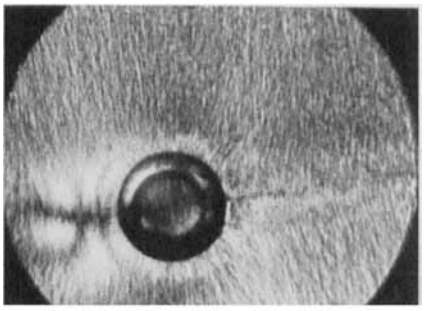

(*b*)

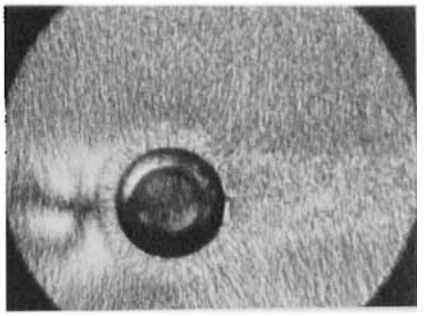

(*c*)

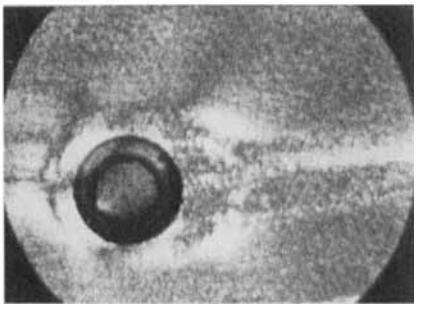

(*d*)

Figure 6. Optical micrographs taken at an intermediate shear rate: $\dot{\gamma}_{xz} = 3\,s^{-1}$. (*a*) During the shear. After stopping the flow, micrographs taken at different times (*b*), (*c*). (*d*) After the bands have vanished.

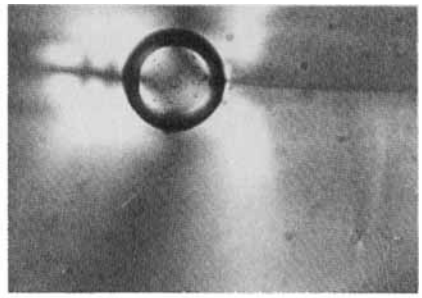

(*a*)

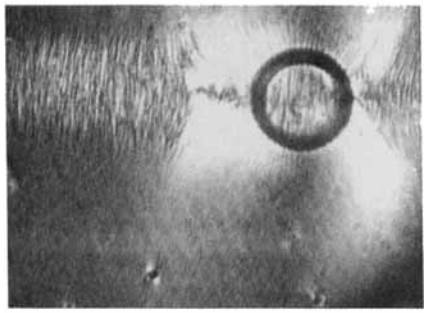

(*b*)

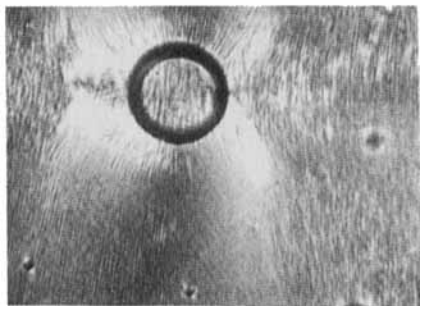

(*c*)

Figure 7. Optical micrographs taken at a high shear rate: $\dot{\gamma}_{xz} = 75\,s^{-1}$. (*a*) During the shear. After stopping the flow, micrographs taken at different times: (*b*) in front of the obstacle, just after stopping the flow; (*c*) some time later.

[15]. The elongation (positive or negative) which occurs around the obstacle and in the wake is probably the driving force which generates the observed bands. After a certain time, the bands vanish but the track of the wake is still visible.

4.3. *Anisotropic solutions: medium cone velocity* ($1{\cdot}1\,s^{-1} \leqslant \dot{\gamma}_{xz} < 50\,s^{-1}$)

All the results described for the low cone velocity are found. The only difference during shear is that the birefringent zone is larger and now has six lobes (figure 6(*a*)). After stopping the flow, the xz shear generates a banded texture in the xy plane which superimposes the previous observed relaxation phenomena (figures 6(*b*), (*c*)) and

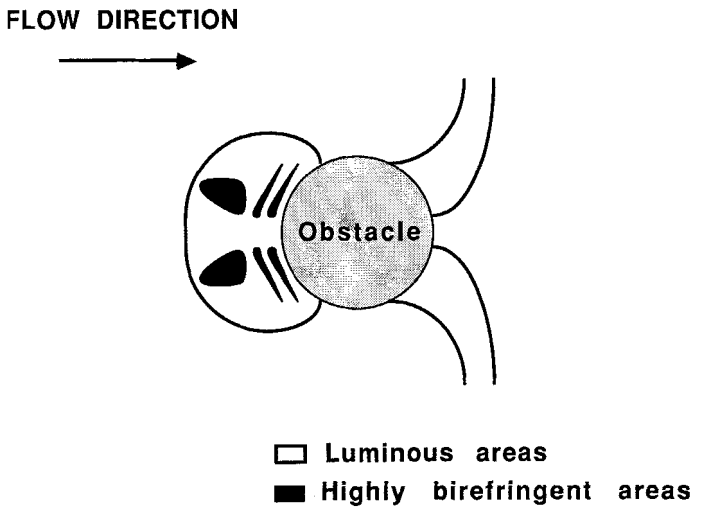

Figure 8. Schematic view of the shear at a high shear rate.

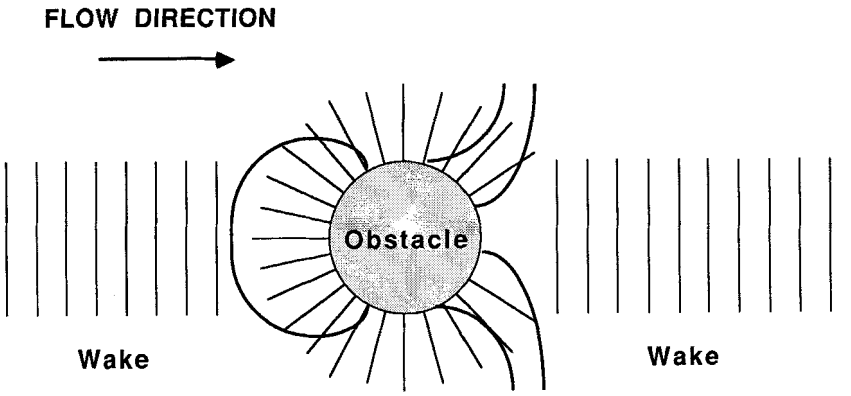

Figure 9. Schematic view showing what is observed after stopping the flow at a high shear rate.

masks the wake. This appears again after some time, when the band texture disappears (figure 6(*d*)).

4.4. *Anisotropic solutions: high cone velocity* ($\dot{\gamma}_{xz} \geqslant 50\,s^{-1}$)

The velocity is such that observations are more difficult to perform. It is nevertheless possible to see that new features appear. First, no eyelashes or chevrons are visible. The six-lobe figure still exists, but we observe two other highly birefringent areas by the rear of the obstacle (figures 7(*a*) and 8). The wake after the obstacle is much smaller in length than at low shear rate, but it is now wider than the obstacle dimensions. A wake is also present in front of the obstacle. After stopping the shear, very fine bands appear in the two wakes in front and at the rear of the obstacle and all around the obstacle as a corona. The corona is larger than at lower shear rates (figures 7(*b*), (*c*) and 9). These zones are very bright. At these high shear rates, the destruction of the bands is very quick. After this, the two wakes are still visible.

5. Conclusion

Anisotropic solutions are already known for their peculiar rheo-optical properties, they also exhibit specific phenomena when perturbed by an obstacle:

(i) streamlines are distorted downstream;
(ii) band textures appear at low velocity around the obstacle and in the wake;
(iii) a very long and persistent wake during shear and after the relaxation is observed;
(iv) a change in the behavior at very high shear rates with the appearance of a wake in front of the obstacle is observed.

These experiments may be relevant to the study of welded flows (behind the obstacle) which is a well-known problem in liquid-crystal polymer processing, resulting in a zone of weakness. We noticed that whatever the shear rate, the weldline (wake) is always present and persists a long time.

We wish to thank H. Maders for the help in the simulation of the flow. This work was supported by grants from the DRET .

References

[1] WISSBRUN, K. F., 1981, *J. Rheol.*, **25**, 601.
[2] KISS, G., and PORTER, R. S., 1980, *J. Polym. Sci. Polym. Phys. Ed.*, **18**, 361.
[3] MOLDENAERS, P., and MEWIS, J., 1986, *J. Rheol.*, **30**, 567.
[4] GOTSIS, A. D., and BAIRD, D. G., 1985, *J. Rheol.*, **29**, 538.
[5] MEWIS, J., and MOLDENAERS, P., 1987, *Molec. Crystals liq. Crystals*, **153**, 291.
[6] NAVARD, P., and ZACHARIADES, A. E., 1987, *J. Polym. Sci. Polym. Phys. Ed.*, **25**, 1089.
[7] ONOGI, S., and ASADA, T., 1980, *Rheology*, Vol. I, edited by G. Astarita, G. Marrucci, L. Nicolais (papers presented at the Eighth International Congress on Rheology, Naples) (Plenum).
[8] METZNER, A. B., and PRILUTSKI, G. M., 1986, *J. Rheol.*, **30**, 661.
[9] HORIO, M., KAMEI, E., and VCHIMURA, H., 1985, *Nikon Reoroji Gakkoishi*, **13**, 25.
[10] ERNST, B., NAVARD, P., and HAUDIN, J. M., 1988, *J. Polym. Sci. Polym. Phys. Ed.*, **26**, 211.
[11] NAVARD, P., and HAUDIN, J. M., 1986, *J. Polym. Sci. Polym. Phys. Ed.*, **24**, 189.
[12] NAVARD, P., 1986, *J. Polym. Sci. Polym. Phys. Ed.*, **24**, 435.
[13] MARSANO, E., CARPANETO, L., and CIFERRI, A., 1988, *Molec. Crystals liq. Crystals*, **158B**, 267.
[14] MARRUCCI, G., 1987, *Proceedings of the International Conference of Liquid Crystal Polymers*, Bordeaux, 20–24 July.
[15] ERNST, B., and NAVARD, P., 1989, *Macromolecules*, **22**, 1419.
[16] ERNST, B., NAVARD, P., HASHIMOTO, T., and TAKEBE, T., *Macromolecules* (in the press).
[17] HASHIMOTO, T., TAKEBE, T., ERNST, B., NAVARD, P., and STEIN, R. S., *J. chem. Phys.* (submitted).
[18] PEUVREL, E., and NAVARD, P., *Macromolecules* (submitted).
[19] TAKAMI, H., and KELLER, H. B., 1969, *Phys. Fluids, Supplement*, **II**, 51.
[20] RAPAPORT, D. C., and CLEMENTI, E., 1986, *Phys. Rev. Lett.*, **57**(6), 695.
[21] TANEDA, S., 1956, *J. phys. Soc. Japan*, **11**(3), 302.
[22] TRITTON, D. J., 1959, *J. Fluid Mech.*, Part 4, 547.
[23] ULTMAN, J. S., and DENN, M. M., 1971, *J. chem. Engng*, **2**, 81.
[24] MENA, B., and CASWELL, B., 1974, *J. chem. Engng*, **8**, 125.
[25] BROADBENT, J. M., and MENA, B., 1974, *J. chem. Engng*, **8**, 11.
[26] JAMES, D. F., and ACOSTA, A. J., 1970, *J. Fluid Mech.*, **42**, 269.
[27] PIAU, J. M., 1974, *C. r. hebd. Séanc. Acad. Sci., Paris*, **278**, 493.
[28] KONIUTA, A., ADLER, P. M., and PIAU, J. M., 1980, *J. non-Newtonian Fluid Mech.*, **7**, 101.
[29] CRESSELY, R., and HOCQUART, R., 1980, *Optica Acta*, **27**, 699.